Free-energy calculations of thermodynamic, vibrational, elastic, and structural properties of α-quartz at variable pressures and temperatures

K. de Boer, A. P. J. Jansen, and R. A. van Santen
Laboratory for Inorganic Chemistry and Catalysis, Eindhoven University of Technology, P.O. Box 513, 5600 MB Eindhoven, The Netherlands

G. W. Watson and S. C. Parker
School of Chemistry, University of Bath, Claverton Down, Bath BA2 7AY, United Kingdom
(Received 11 July 1995; revised manuscript received 21 February 1996)

The reliability of two shell model potentials and a rigid-ion model potential has been investigated by comparing available experimental data with predicted values for a large number of α-quartz properties at variable temperatures and pressures. Calculations were done with a recently developed free-energy minimization code. Predictions for the structure, Raman modes, and elastic constants of α-quartz at elevated temperatures and pressures are discussed. Calculations of the constant pressure entropy and heat capacity as a function of temperature are presented. Calculated low-frequency phonon dispersion curves in the $[\xi\ \xi\ 0]$, $[\xi\ 0\ 0]$, and $[0\ 0\ \xi]$ direction are also discussed. Analysis of these predictions shows which atomic interactions are most accurately described by each potential. Furthermore, the conditions are discussed under which the predictions of each potential are the most reliable. [S0163-1829(96)00226-3]

I. INTRODUCTION

From a technological point of view, silicon dioxide is an interesting material. It is used in many electronic devices, as well as in the ceramic industry and the synthesis of zeolites. Zeolites are microporous materials that, in general, have complex structures. These materials are mainly used as detergents and catalysts in many industrial processes. Therefore, a large number of approaches has been developed to predict all-silica structures and their properties. These approaches range from *ab initio* quantum mechanical calculations[1–9] to those based on interatomic potentials.[10–13] Although *ab initio* calculations give more accurate results than the semiempirical potentials reported so far,[4–7] they are computationally expensive. Intrinsic complexity of a crystalline solid, i.e., a low symmetry or a large unit cell, can make an *ab initio* calculation computationally intractable.[4] The use of interatomic potentials might then be desirable, provided that they are sufficiently accurate. Therefore, the development of reliable interatomic potentials, especially those derived from *ab initio* data, is a subject of interest. It is also useful to know how reliable the interatomic potentials are under different conditions.

In this work, we have investigated the reliability of a recently derived *ab initio* shell model potential[10] and two other interatomic potentials.[11,12] This is done by making detailed comparisons between predicted and experimental values for a large number of α-quartz properties at variable temperatures and pressures. Calculations were done with the free energy minimization code PARAPOCS.[14] We will discuss predictions for the structure, Raman modes, and elastic constants of α-quartz at elevated temperatures and pressures. We will consider predictions for the temperature dependence of the constant-pressure entropy and heat capacity of α-quartz. Calculated low-frequency phonon dispersion curves in the $[\xi\ \xi\ 0]$, $[\xi\ 0\ 0]$, and $[0\ 0\ \xi]$ direction will also discussed. Analysis of these predictions will demonstrate which atomic interactions are the most accurately described by each potential. We will further indicate under which conditions the predictions of each potential are the most reliable.

II. COMPUTATIONAL DETAILS

Free-energy minimizations were done with the code PARAPOCS,[14] which can be used to calculate physical properties of solids at variable temperatures and pressures. To calculate thermodynamical properties, the vibrational frequencies of the solid must be computed. The calculations assume that vibrational motions in the solid are described by independent quantized harmonic oscillators. The frequency of those oscillators varies with cell volume.[15] Minimization of the Gibbs free energy can be achieved by varying the cell volume and the positions of the ions until the configuration satisfies the following equilibrium conditions at a given temperature and pressure:

$$\frac{\partial A}{\partial V} = P_{\mathrm{app}}, \tag{1}$$

$$\frac{\partial U_{\mathrm{stat}}}{\partial \mathbf{r}} = 0. \tag{2}$$

In Eq. (1) A denotes the Helmholz free energy, V the cell volume, and P_{app} the applied pressure. In Eq. (2) U_{stat} denotes the static energy due to the interatomic interactions and $\mathbf{r}$ denotes the atomic coordinates. Equation (1) states that the pressure exerted by the system (internal pressure) must equal the applied pressure. [Equation (1) is only valid for cubic crystals. For more general cases the derivatives of the Gibbs free energy with respect to the strain must be computed. Details can be found in Ref. 16.] Equation (2) states that the net force on each atom must vanish. After the Gibbs free energy is minimized, thermodynamical properties, elastic constants, dielectric constants, and the structure of the solid

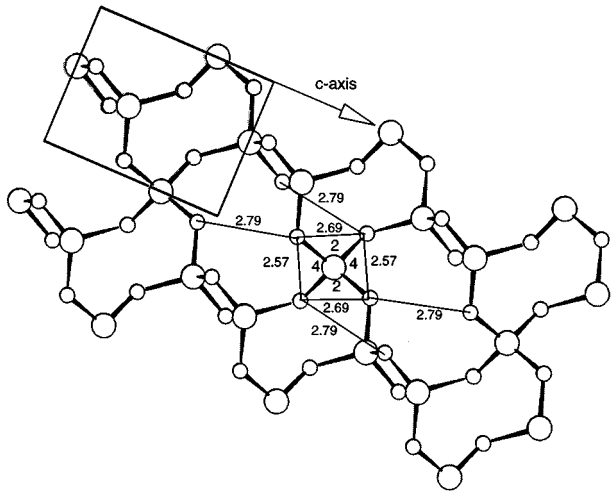

FIG. 1. Intratetrahedral distances, OO_s distances, and tetrahedral angles in the experimental structure of α-quartz at $P=10.2$ GPa (Ref. 21) viewed along the a axis. Distances of 2.79 Å are the OO_s distances. Numbering of the tetrahedral angles corresponds to that in Fig. 3. Numbers 2 and 4 denote tetrahedral angles in the plane of drawing. Angles 1 and 3 in Fig. 3 are perpendicular on the plane of drawing.

can be computed. Calculation of the Helmholz free energy and other thermodynamical properties requires computation of the vibrational frequencies for all wave vectors in the Brillouin zone. Those frequencies are calculated with an appropriate wave vector grid. (See the Appendix.)

In our calculations we have employed the recently derived *ab initio* shell model potential of de Boer *et al.*[10] denoted as the BJS (de Boer–Jansen–van Santen) potential. We have used the shell model potential published by Catlow *et al.*[11] and the rigid-ion model potential derived by Kramer *et al.*[12] The latter potentials are referred to as the JC (Jackson-Catlow) and KFBS (Kramer-Farragher–van Beest–van Santen) potential, respectively. Cutoffs applied in calculations using the KFBS and JC potential are 10 Å.[17] The covalent OO interactions of the BJS potential are applied with a cutoff of 3.5 Å, because for larger distances all covalent terms are effectively zero. The covalent SiO interaction of this potential is applied with a cutoff of 2.5 Å (i.e., in between the nearest and next nearest Si and O neighbors) to simulate a real Si-O bond. The electrostatic interactions are calculated using the Ewald summation.

III. CALCULATIONS OF α-QUARTZ AT VARIABLE PRESSURES

A. Pressure-induced changes of the α-quartz structure

We will first review the pressure-induced geometrical changes of α-quartz that are known from experiment.[18–21] These changes and their correlations are important in our subsequent discussion. Compression of α-quartz is mainly governed by changes in the bond angles because the Si-O bond distances remain virtually constant at variable pressures.[18–21] Therefore, we will concentrate on changes of the bond angles with pressure. Figure 1 shows the experimental structure of α-quartz at $P=10.2$ GPa. At low pressure, the compression of α-quartz is governed by decrease of the weak Si-O-Si bond angle, together with rotation of the tetrahedra along their twofold axis perpendicular to the c axis.[18–21] The pressure-induced decrease of the Si-O-Si bond angle and that of the smallest intertetrahedral distance are correlated. This distance will be referred to as the OO_s distance. Decreased OO_s distances caused increased OO repulsions. (See Fig. 1.) The increased OO repulsions cause distortion of the tetrahedral O-Si-O bond angles. The tetrahedral bond angles do not change much at low pressures, because they are more rigid than the Si-O-Si bond angles.[18–21] The tetrahedral bond angles become gradually more distorted when pressure is increased. The decrease of the Si-O-Si bond angle becomes less pronounced at higher pressures. The tetrahedral bond angle distortion is therefore mainly responsible for the compression of α-quartz at high pressures. Unit cell compression of α-quartz is directly related with compression of the intertetrahedral distances, which are themselves related to the bond angle compression.[18] The c-axis compression is correlated with changes of the OO_s distance, because this distance has the largest component parallel to the c axis.[21] The c-axis compression is via the OO_s distance correlated to compression of the Si-O-Si bond angle. Compression of the a axis is correlated with that of the OO_l distance (the largest intertetrahedral distance) because one of these two distances is nearly parallel to the a axis. The other is approximately 45° between a and c.[19]

The calculated and experimental α-quartz structures at ambient conditions are given in Table I. Table II presents predictions for the Si-O bond distances in α-quartz at variable pressures. All potentials predict that the Si-O bond distances in α-quartz change slightly with pressure, which is in accordance with experiment. Hence, we will focus on predictions of the bond angle compression of α-quartz. Furthermore, all results are obtained for pressures up to the value at which each potential predicts acoustic mode softening. This will be further discussed in Sec. III A. Calculated and experimental[18,20,21] values for the compression of the Si-O-Si bond angle and c axis are shown in Figs. 2 and 3. Although the JC-predicted α-quartz structure at ambient conditions is the closest to experiment, this potential slightly underestimates the Si-O-Si bond angle at any pressure. Predictions of

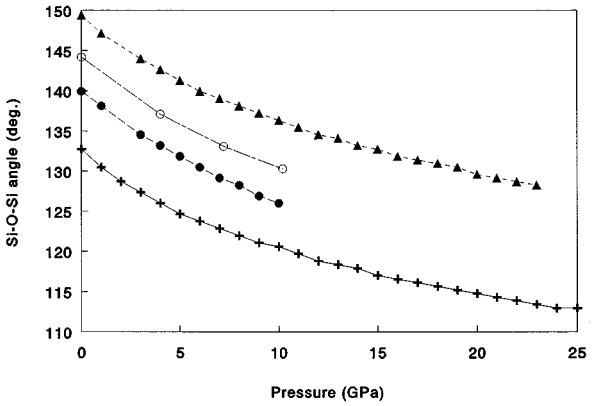

FIG. 2. Predictions for the Si-O-Si bond angle in α-quartz versus pressure, compared with experimental data of Glinneman *et al.* (Ref. 21). Crosses: BJS predictions. Closed triangles: KFBS predictions. Closed points: JC predictions. Open points: data of Glinneman *et al.* (Ref. 21).

TABLE I. Predictions for the structure of α-quartz at $T=300$ K compared with experiment (Ref. 28). Distances are in Å and angles in degrees.

	Expt	BJS	KFBS	JC
$d_{\text{Si-O}_l}$	1.614	1.623	1.606	1.614
$d_{\text{Si-O}_s}$	1.606	1.620	1.598	1.607
a	4.91	4.77	4.96	4.85
c	5.41	5.23	5.47	5.36
∠Si-O-Si	143.6	132.8	149.6	140.0
$\angle\text{O-Si-O}_1$	109.3	108.9	110.4	109.5
$\angle\text{O-Si-O}_2$	110.5	112.8	107.7	111.2
$\angle\text{O-Si-O}_3$	108.9	104.4	114.9	108.2
$\angle\text{O-Si-O}_4$	108.8	108.9	108.1	108.4

the JC potential for the Si-O-Si bond angle, OO_s distance, and c axis at low pressures are in agreement with the experimental correlation mentioned earlier. (See Figs. 2 and 3. The predicted OO_s distance follows a trend similar to that of the c axis with pressure.) Hence the underestimation of the OO_s distance at low pressures might be caused by underestimation of the Si-O-Si bond angle, insufficient OO repulsions, or a combination of both. To investigate this, we have studied pressure-induced changes of the a axis, OO_l distance, and O-Si-O bond angles. As explained above, those properties are virtually independent of the Si-O-Si bond angle. The JC predictions of the OO_l distance and a axis versus pressure reproduce the experimental curve. (The latter quantities are underestimated by 4% and 1%, respectively.) Thus the OO interactions at longer interatomic distances are reasonably described. Figure 4 illustrates calculated and experimental values for the tetrahedral bond angles at variable pressures. Those angles are well predicted by the JC potential. This could be expected because the JC potential contains, besides an OO pair potential term, an O-Si-O bending term, in contrast to both other potentials. Therefore, the underestimation of the Si-O-Si bond angle is mainly responsible for that of the OO_s distance and c axis at low pressure. At higher pressures, the predicted OO_s distance and c axis become increasingly too low. We attribute this to an underestimation of the OO repulsions at *short* interatomic distances because the difference between predicted and experimental values for the Si-O-Si bond angle is nearly constant in the pressure range studied. (See Figs. 2 and 3.)

We conclude that the electrostatic interactions in the JC potential, which determine the Si-O-Si bond angle, are slightly too weak and that the OO repulsions at short interatomic distances are underestimated.

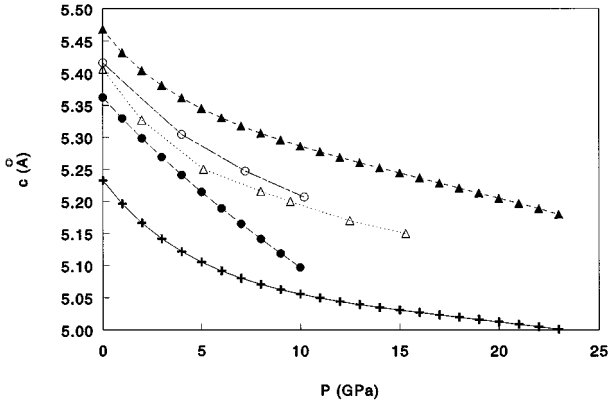

FIG. 3. Predictions for the c axis in α-quartz versus pressure, compared with experimental data of Hazen *et al.* (Ref. 18) and Glinneman *et al.* (Ref. 21). Crosses: BJS predictions. Closed triangles: KFBS predictions. Closed points: JC predictions. Open triangles: data of Hazen *et al.* (Ref. 18). Open points: data of Glinneman *et al.* (Ref. 21).

The KFBS predictions for the α-quartz structure at variable pressures are less accurate than those of the JC potential. This is mainly caused by overestimation of the Si-O-Si bond angle as will be shown next. The KFBS-predicted values of the OO_s distance and c axis, which are too large, are consistent with overestimation of the Si-O-Si bond angle. (See Figs. 2 and 3.) Predictions for the OO_l distance and a axis, properties that are mainly determined by the OO potentials, follow the experimental trend. (At variable pressures, the latter quantities are overestimated by 2% and 1%, respectively.) The KFBS potential predicts the tetrahedral bond angles in α-quartz less accurate than the JC potential. (See Fig. 4.) However, KFBS predictions for the angles which vary the most under pressure follow the experimental trend. The discrepancy between the KFBS-predicted structure and experiment is therefore mainly due to overestimation of the Si-O-Si bond angle.

We conclude that the electrostatic interactions in the KFBS potential, which determine the Si-O-Si bond angle, are too stiff.

The BJS prediction for the structure of α-quartz at variable pressures is less accurate than that of both other potentials. This is mainly due to underestimation of both the Si-O-Si bond angle and the OO repulsions, as will be shown next. The BJS potential underestimates the Si-O-Si bond

TABLE II. Predictions for Si-O bond distances in α-quartz versus pressure at $T=300$ K, compared with experiment (Ref. 21). P denotes pressure, r_l the longest Si-O bond distance, and r_s the shortest Si-O distance. Distances are in Å and pressures in GPa. Distances in the third row are the predicted values at pressures which induce acoustic mode softening.

	Expt.		BJS		KFBS		JC	
P	r_l	r_s	r_l	r_s	r_l	r_s	r_l	r_s
0.0	1.614	1.606	1.623	1.620	1.606	1.598	1.614	1.607
9.5	1.621	1.596	1.639	1.639	1.598	1.580	1.627	1.605
			1.652	1.639	1.594	1.570	1.627	1.605

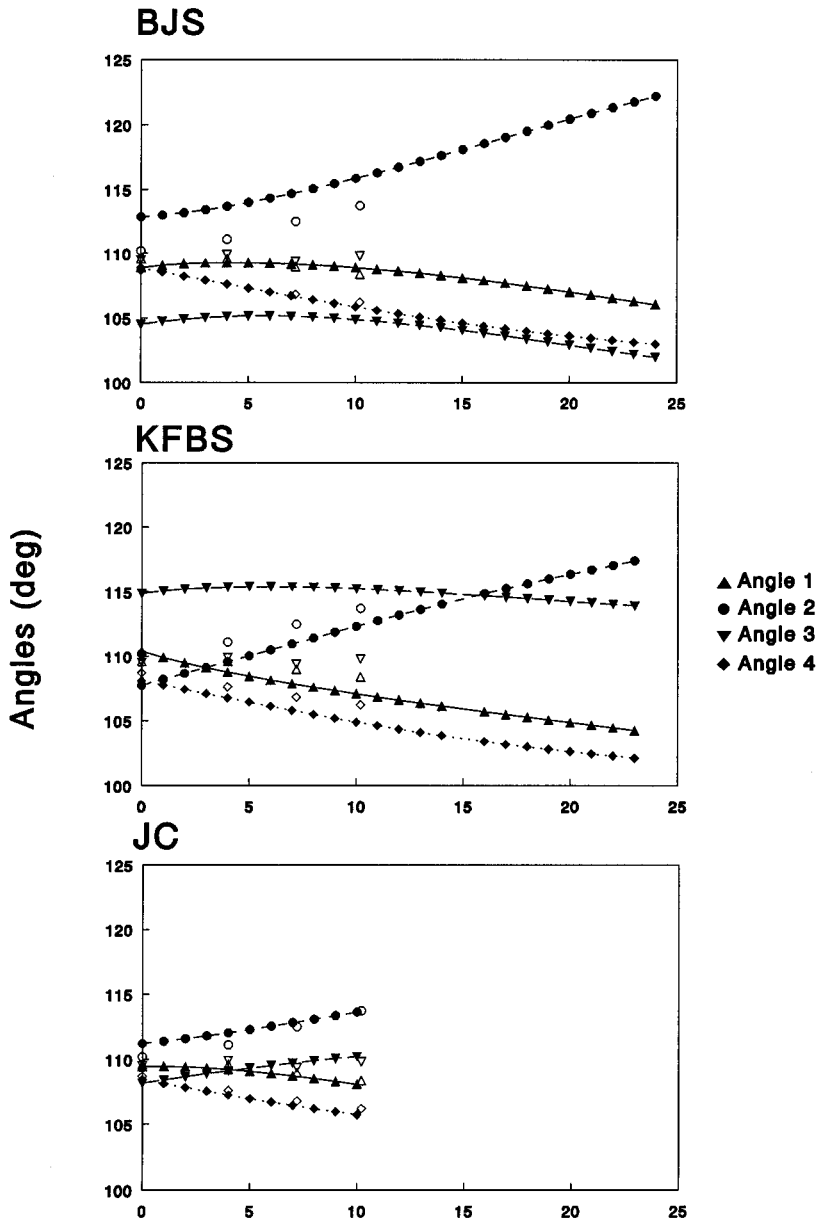

FIG. 4. Predictions for the tetrahedral angles in α-quartz versus pressure, compared with experimental data of Glinneman *et al.* (Ref. 21). Closed symbols: calculations. Open symbols: experiment. The numbering of angles is identical to that in Fig. 1.

angle at any pressure. The same holds for the predicted *c* axis and OO_s distance. (See Figs. 2 and 3. The OO_s distance is underestimated by 10% at any pressure.) Predicted values for the OO_l distance and *a* axis are 7% and 3% too low, respectively. This indicates that the OO repulsions are too weak. These weak OO repulsions might also be responsible for the less accurate prediction of the tetrahedral bond angles. (See Fig. 4.)

We conclude that the electrostatic interactions in the BJS potential, that determine the Si-O-Si bond angle, are too weak. This potential also underestimates the OO repulsions.

How the above discussed deficiencies of each potential affect predictions for a large range of other physical properties will be discussed in the remaining sections.

B. Mechanical properties and acoustic modes of α-quartz

When α-quartz is subjected to high pressure, one of its acoustic modes becomes soft. Softening of an acoustic mode with a wave vector close to the Γ point indicates elastic instability of the material, caused by violation of the Born stability criteria.[3,22] Softening on other special points in the Brillouin-zone indicates formation of a supercell.[5,23,24] The x-ray-diffraction measurements of Kingma *et al.*[25–27] indicate that α-quartz forms a $3\times3\times1$ supercell at $P=21$ GPa. This supercell is created by tripling of the unit cell in the *a* and *b* directions of α-quartz and is consistent with acoustic mode softening along $[\xi\ \xi\ 0]$ at the *K* point.[23] According to Kingma *et al.*,[25] α-quartz becomes gradually amorphous (i.e., the sample contains both crystalline and amorphous SiO_2) at pressures between 21 and 30 GPa. The material becomes completely amorphous at $P=30$ GPa.[25] Other reported amorphization pressures range from 15 (Ref. 18) to 35 GPa.[29] The amorphization of α-quartz is subject to debate. According to some authors,[3,5,13] amorphization starts at the pressure which induces softening of acoustic modes close to the Γ point, indicating mechanical instability.[22] Others[30] suggest that amorphization immediately happens after for-

mation of the $3\times3\times1$ supercell, just above the pressure that induces mode softening at the K point. Amorphization of α-quartz would then be due to dynamic instability[30] prior to the mechanical instability. In this paper, we will compare experimental amorphization pressures with calculated pressures that induce acoustic mode softening close to the Γ point.

The JC potential predicts that the lowest acoustic branch along $[0\ 0\ \xi]$ softens at the A point when α-quartz is subjected to a pressure of 9.6 GPa. This prediction indicates formation of a supercell that is *different* from the $3\times3\times1$ structure reported by Kingma *et al.*[25] We will show that this discrepancy is due to underestimation of both the Si-O-Si bond angle and the OO repulsions at short interatomic distances. At pressures slightly above 9.6 GPa, the JC potential predicts imaginary frequencies close to the Γ point for phonons along $[0\ 0\ \xi]$, indicating that the structure becomes mechanically unstable. The mechanical stability of α-quartz is determined by the Born stability criteria $B1$, $B2$, and $B3$.[31] Terhune *et al.*[31] derived the directions along which acoustic mode softening must occur in order to violate these criteria. The JC-predicted mode softening along $[0\ 0\ \xi]$ does *not* agree with any of those directions. Thus the JC predicted supercell formation is not accurate, because it is due to mode softening along the $[0\ 0\ \xi]$ direction. This leads to an instability that is inconsistent with violation of the Born stability criteria. The instability along $[0\ 0\ \xi]$ indicates that the stiffness of the crystal in the c direction is underestimated. At pressures well above 9.6 GPa, the JC potential predicts that the next branch which softens is the lowest acoustic branch along $[\xi\ \xi\ 0]$. At $P=16.8$ GPa, this branch softens at the K point. At higher pressures, the JC potential predicts imaginary frequencies close to the Γ point for phonons propagating along $[\xi\ \xi\ 0]$. These results would be consistent with formation of the $3\times3\times1$ supercell at $P=16.8$ GPa, followed by violation of the $B3$ stability criterion at a higher pressure. Thus the weakness of the c axis is responsible for softening of the lowest acoustic branch along $[0\ 0\ \xi]$ before softening of modes with wave vectors along the correct $[\xi\ \xi\ 0]$ direction can take place. This underestimated stiffness of the crystal in the c direction is due to underestimation of both the Si-O-Si bond angle and the OO repulsions at short interatomic distances, as argued in Sec. III A. That the JC potential is less appropriate for studies of the mechanical properties of α-quartz under pressure is further indicated by less precise predictions for the pressure shifts of the elastic constants. The pressure shift of an elastic constant is defined as the derivative of this constant with respect to pressure at $P=0$. Table III gives predicted and experimental values for the pressure shifts.

The BJS potential predicts that the lowest acoustic branch along $[\xi\ \xi\ 0]$ softens in the vicinity of the Γ point when α-quartz is subjected to a pressure of 24.2 GPa. This value is comparable to experimental amorphization pressures (see above) and the predicted mode softening agrees with violation of the $B3$ stability criterion. However, at pressures below 24.2 GPa, no mode softening at the K point is predicted. Thus the BJS potential only predicts the pressure-induced elastic instability of α-quartz without prior formation of the $3\times3\times1$ superstructure. Thus, although the structure of α-quartz is predicted less properly, the BJS potential is still able to model the mechanical properties of this material under pressure. This can be explained as follows. Recall that the BJS-predicted c axis is systematically too low at all pressures due to underestimation of the Si-O-Si bond angle. Weak OO repulsions are mainly responsible for the underestimated value of the a axis. (See Sec. III A.) As the BJS potential underestimates both axes, their ratio can still be accurate. The BJS predicted c/a ratio is closest to that determined by experiment[18,21] at moderate and high pressures. Experimental, KFBS, JC, and BJS values for this ratio at $P=9.5$ GPa are 1.131, 1.139, 1.122, and 1.129, respectively. Experimental, KFBS and BJS values for the c/a ratio at $P=15.3$ GPa are 1.152, 1.162, and 1.154, respectively. The accurate BJS prediction of the c/a ratio indicates a balance in the forces along the c and a direction. This enables the BJS potential to model the mechanical properties of α-quartz under pressure, although the structure of this material is predicted less properly. That the BJS potential is suitable for modeling the mechanical properties of α-quartz is further indicated by reasonable predictions for the pressure shifts of the elastic constants. (See Table III.)

TABLE III. Predictions for pressure shifts of the elastic constants of α-quartz, compared with experimental data of McSkimin *et al.* (Ref. 45) and Wang *et al.* (Ref. 46). Elastic constants are denoted as C_{ij}.

C_{ij}	McSkimin	Wang	BJS	KFBS	JC
C_{11}	3.82	1.49	1.65	1.38	−1.12
C_{12}	8.66	12.12	5.54	7.68	4.61
C_{13}	5.97	4.04	4.63	6.67	2.27
$\lvert C_{14}\rvert$	1.93	3.96	1.73	1.83	1.26
C_{33}	10.84	9.51	11.50	14.79	1.94
C_4	2.66	1.84	−1.08	1.76	−2.14
C_{55}	−2.96	−5.32	−1.95	−3.15	−2.86

The KFBS potential predicts that the lowest acoustic branch along the $[\xi\ \xi\ 0]$ direction of α-quartz becomes soft at the K point when pressure is increased to 22.8 GPa. The predicted mode softening is consistent with formation of the $3\times3\times1$ superstructure, reported by Kingma *et al.*[25] At higher pressures [25 GPa at $T=0$ (Ref. 30)], the KFBS potential predicts imaginary frequencies for phonons with wave vectors along $[\xi\ \xi\ 0]$ which are close to the Γ point. This is consistent with violation of the $B3$ stability criterion. That the KFBS potential is appropriate for modeling the mechanical properties of α-quartz under pressure is further indicated by accurate predictions for the pressure derivatives of the elastic constants. (See Table III.) The good KFBS predictions for the mechanical properties of α-quartz at high pressures are not inconsistent with less accurate predictions for the structure. We recall from Sec. III A that the KFBS potential overestimates the Si-O-Si bond angle, causing the predicted crystal to be too stiff in the c direction. The KFBS-predicted c/a ratio (see above) is slightly too high. Thus the predicted crystal is relatively too weak in the a direction. This favors the instability along the $[\xi\ \xi\ 0]$ direction, leading to violation of the $B3$ stability criterion.

C. Low-frequency Raman modes of α-quartz

We will consider the low-frequency Raman modes and their pressure shifts because they are the most sensitive to

TABLE IV. Predictions for frequencies and pressure shifts (latter in parenthesis) of the six lowest Raman modes of α-quartz, compared with experiment (Ref. 34). Calculations are done using $\mathbf{k}\rightarrow 0$ along the c axis. Calculations with $\mathbf{k}\rightarrow 0$ along the a axis gave similar results. Frequencies are in cm^{-1} and pressure shifts in $cm^{-1}\,kbar^{-1}$.

Expt.	BJS	KFBS	JC	Symmetry
128 (0.54)	125 (0.35)	165 (0.57)	143 (0.50)	E(TO+LO)
206 (2.04)	227 (1.25)	226 (2.61)	222 (1.72)	A1
464 (0.81)	426 (1.21)	585 (0.19)	463 (0.82)	A1
696 (0.80)	695 (0.35)	718 (0.53)	717 (0.46)	E(TO+LO)
796 (0.59)	801 (0.50)	761 (0.91)	821 (0.57)	E(TO)
808 (0.59)	801 (0.50)	761 (0.91)	821 (0.57)	E(LO)

pressure.[32–35] The pressure shift of a mode is defined as the derivative of the frequency with respect to pressure at $P=0$. As low-frequency Raman modes are sensitive to temperature changes,[35] we have done the calculations at $T=300$ K. For predictions of the high-frequency Raman modes we refer to $T=0$ calculations in literature[10,32,33] as, according to experiment[35] and to our calculations, temperature effects are negligible for those modes.

Table IV presents predicted and experimental[34] values for the low-frequency Raman modes of α-quartz at ambient conditions. The JC predictions for those modes and their pressure shifts are accurate. This is consistent with good JC predictions for properties of α-quartz at zero pressure, as discussed previously. This also indicates that temperature effects are accurately predicted by the JC potential. The BJS predictions for the low-frequency Raman modes are accurate, except that the experimental 464 cm^{-1} mode is underestimated. The BJS-predicted atomic displacements of this mode show a symmetrical Si-O-Si bond angle stretch along the Si-O bonds, which agrees with experiment.[34] The underestimated frequency of the latter mode indicates that the predicted stretch is too weak. This is due to the predicted Si-O-Si bond angle, which is too narrow, because in silicates there exists a negative coupling between the Si-O bond distance and the Si-O-Si bond angle.[36] Consequently, the Si-O bond distance is slightly overestimated. (See Tables I and II.) The overestimated pressure shift of the experimental 464 cm^{-1} mode further indicates that the interactions in the BJS potential which determine the Si-O-Si bond angle are too weak. The other modes and their pressure shifts are accurately predicted, although the calculated α-quartz structure is less close to experiment. As for the BJS results, discussed earlier, this is due to underestimation of both the Si-O-Si bond angle and the OO repulsions. This can be seen as follows. Atomic displacements of the BJS-calculated 125 cm^{-1} mode correspond with rotation of the tetrahedra around their twofold axis perpendicular to the c axis. The rotation of the tetrahedra is caused by OO repulsions along the OO_s distances. (See Fig. 1.) We recall that the Si-O-Si bond angle and the correlated OO_s distance in α-quartz are underestimated by the BJS potential. This would cause an overestimation of OO repulsions along the OO_s distances. The latter would facilitate an easy rotation of the tetrahedra, leading to an underestimation of the frequency. The fact that this does not happen indicates that the OO repulsions must be too weak. Thus the weak OO repulsions compensate for the too small value of the Si-O-Si bond angle. Atomic displacements of the other modes are complex and show changes in the Si-O-Si bond angle and distortion of O-Si-O angles. The accurate prediction of those modes might also be due to the above mentioned compensation effect. At high pressure, the experimental 577 cm^{-1} mode, which corresponds to the symmetrical Si-O-Si bond angle stretch, is underestimated while the two lowest Raman modes are predicted accurately. (See Table V.) Thus, also at elevated pressure, the underestimated Si-O-Si bond angle is compensated by weak OO interactions.

TABLE V. Predictions of the six lowest Raman modes of α-quartz at $P=20$ GPa and $T=300$ K, compared with experiment (Ref. 34). Calculations are done using $\mathbf{k}\rightarrow 0$ along the c axis. Calculations with $\mathbf{k}\rightarrow 0$ along the a axis gave similar results. Frequencies are in cm^{-1}.

Expt.	BJS	KFBS	Symmetry
165	165	242	E(TO+LO)
311	308	348	A1
577	551	651	A1
793	720	825	E(TO+LO)
895	838	874	E(TO)
895	838	874	E(LO)

We recall that the KFBS potential overestimates the Si-O-Si bond angle. This is clearly reflected in the calculated low-frequency Raman modes and their pressure shift. (See Table IV.) Overestimation of the experimental 464 cm^{-1} mode is consistent with overestimation of the Si-O-Si bond angle; for the same reasons explained for the BJS potential. Consequently, the predicted pressure shift of this mode is too low. Overestimation of the experimental 128 cm^{-1} mode reflects a hindered rotation of the tetrahedra. This is due to overestimation of the Si-O-Si bond angle and the correlated OO_s distance. The latter causes OO repulsions which are too weak. We notice that the overestimated stiffness of the Si-O-Si bond angle is less apparent in predictions for the higher frequency modes. (See Table IV.) The same trend is reflected at higher pressures. (See Table V.)

We have discussed the relation between potential parameters and predicted properties of α-quartz at variable pressures. How these parameters affect predictions of temperature dependent properties will be discussed below.

IV. CALCULATIONS OF α-QUARTZ AT VARIABLE TEMPERATURES

A. Temperature-induced changes of the α-quartz structure

Experiments[21,28] indicate that the α-quartz structure changes slightly upon heating. According to experiment,[28] the Si-O-Si bond angle increases by 2.5° in the range 300–813 K. The BJS, KFBS, and JC-predicted values for this change are 2.3°, 1.4°, and 0.9°, respectively. All potentials predict that the largest change of the tetrahedral angles is less than one degree in the range 300–813 K, which agrees with experiment.[28] Table VI shows predicted and experimental values for the Si-O bond distances in α-quartz at elevated temperatures. Only the BJS potential predicts that both Si-O

TABLE VI. Predictions for Si-O bond distances in α-quartz for several temperatures compared with experiment (Ref. 28). T denotes temperature, r_l the longest, and r_s the shortest Si-O bond distance. Distances are in Å and temperatures in K.

	Expt.		BJS		KFBS		JC	
T	r_s	r_l	r_s	r_l	r_s	r_l	r_s	r_l
300	1.605	1.614	1.620	1.622	1.598	1.606	1.607	1.614
813	1.600	1.594	1.618	1.621	1.600	1.606	1.608	1.614

bond distances decrease in the temperature range studied. This agrees with the experimental trend.

The mechanical properties of α-quartz do not show a strong temperature dependence in the temperature range studied. Table VII gives calculated and experimental values for the elastic constants of α-quartz at variable temperatures. All three potentials give accurate predictions for those constants. Thus the potentials predict that temperature-induced changes of the elasticity and structure of α-quartz are small. This is in accordance with experiment. Therefore, the accuracy of the predicted structure and elasticity of α-quartz at elevated temperatures is mainly determined by the performance of the potentials at ambient conditions. The latter was discussed in Sec. III.

B. Thermodynamics and phonon dispersion curves of α-quartz

We have studied low-frequency phonon dispersion curves because these phonons mainly determine the thermodynamic properties. Figures 5–7 illustrate calculated and experimental phonon dispersion curves of α-quartz at $T=20$ and 300 K. Calculations at $T=800$ K indicate that the phonon dispersion curves at α-quartz virtually do not change with temperature. We can thus relate the accuracy of the predicted thermodynamic properties at any temperature to that of the phonon dispersion curves in Figs. 5–7. The JC potential gives the most accurate prediction for the phonon dispersion curves. Consequently, the thermodynamic properties of α-quartz are accurately predicted. The JC prediction for the constant-pressure entropy differs by 1% from the experimental value[37,38] for temperatures between 200 and 800 K. Also, the JC prediction of the constant-pressure heat capacity is accurate for temperatures up to 700 K. Figure 8 illustrates calculated and experimental heat capacities. We notice that all predicted values for the heat capacity show similar deviations from experiment at temperatures above 700 K. This is perhaps caused by the semiharmonic calculations, which cannot cope with the α-quartz$\rightarrow\beta$-quartz transition, instead of inaccuracies in the parameter sets.

The accuracy of the BJS-predicted phonon dispersion curves is almost comparable to that of the JC potential. (See Figs. 5 and 6.) Thus the less accurate BJS prediction for the structure of α-quartz is virtually not reflected in the calculated phonon dispersion curves. This is consistent with our discussion on the Raman results. (See Sec. III C.) The BJS prediction of the constant-pressure heat capacity is accurate. (See Fig. 8). The constant-pressure entropy is overestimated by 7%, which seems reasonable. The KFBS potential overestimates the optic branches in the phonon dispersion diagram. (See Fig. 7.) This must be due to the Si-O-Si bond angle that is overestimated, as shown in our discussion on the Raman results. (See Sec. III C.) Consequently, the constant-pressure entropy and heat capacity are systemati-

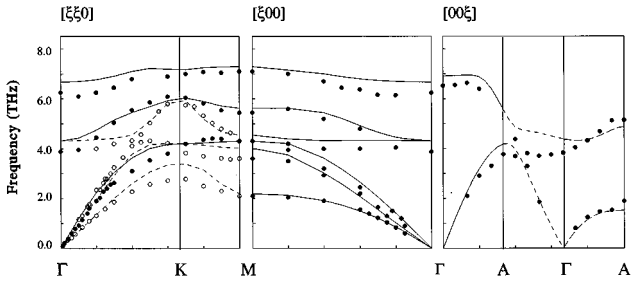

FIG. 5. Low-frequency phonon dispersion curves in the main directions of α-quartz as predicted by the JC potential in comparison with experiment. The $[\xi\,\xi\,0]$ and $[\xi\,0\,0]$ direction are measured by Dorner *et al.* at $T=300$ K (Ref. 48) and calculations are done at $T=300$ K. The $[0\,0\,\xi]$ direction is measured by Strauch *et al.* (Ref. 49) at $T=20$ K and calculations are done at 0 K. Lines: calculations. Points: measurements. In $[\xi\,\xi\,0]$ direction: open points and broken lines show the $T2$ representation; closed points and straight lines show the $T1$ representation. For the $[0\,0\,\xi]$ direction an extended zone scheme is used.

TABLE VII. Predictions for elastic constants of α-quartz at several temperatures compared with experiment (Ref. 47). Elastic constants are denoted as C_{ij} and are in GPa.

$T=300$ K				
C_{ij}	Expt.	BJS	KFBS	JC
C_{11}	84.84	87.78	89.63	95.25
C_{12}	5.31	13.82	3.96	16.21
C_{13}	12.24	9.18	11.68	18.63
C_{14}	−17.66	−18.20	−18.50	−15.08
C_{33}	105.44	107.20	99.55	115.17
C_{44}	57.55	55.12	49.22	51.00
C_{66}	39.77	36.98	42.83	39.51
$T=400$ K				
C_{ij}	Expt.	BJS	KFBS	JC
C_{11}	84.18	87.64	89.51	95.38
C_{12}	3.42	13.13	3.01	15.75
C_{13}	11.20	8.68	10.90	18.42
C_{14}	−17.72	−18.39	−18.66	−15.19
C_{33}	103.18	105.77	97.90	114.98
C_{44}	56.92	55.23	48.97	51.19
C_{66}	40.38	37.25	43.25	39.82

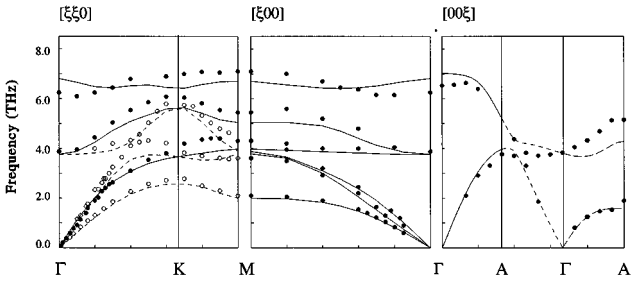

FIG. 6. Low-frequency phonon dispersion curves in the main directions of α-quartz as predicted by the BJS potential in comparison with experiment. Experimental data, temperatures for which the calculations are done, and symbols are the same as in Fig. 5.

cally underestimated. (See Fig. 8. The entropy is underestimated by 12%.) Gonze *et al.* have reported first-principles calculations of the phonon dispersion curves[7] and the constant-volume heat capacity[8] of α-quartz, that are in better agreement with experiment than the predictions of the BJS and JC potential. Given the simplicity of the latter calculations compared to that of the *ab initio* calculations, we consider the predictions of the BJS and JC potential to be very reasonable. Gonze *et al.*[7–9] compared the interatomic force constants, calculated with the KFBS potential, with those obtained from the *ab initio* calculations. They suggest that two-body potentials are less suitable for a detailed description of the lattice dynamics of α-quartz. They advocate the use of three-body potentials. In this work we have shown that the JC potential, which contains a three-body term, indeed gives better predictions than the KFBS potential for the phonon dispersion curves of α-quartz.

V. CONCLUSIONS

A. The JC potential

The JC potential can model low-frequency Raman spectra and phonon dispersion curves of α-quartz at zero pressure. Good predictions are also given for the structure and the elasticity at zero pressure. Thermodynamic properties and the structure of α-quartz at variable temperature are accurately predicted. The JC potential is not able to model properties of α-quartz at pressures above $P=9.6$ GPa. This is due to a predicted acoustic mode softening which is not in accordance with violation of the Born stability criteria. The less

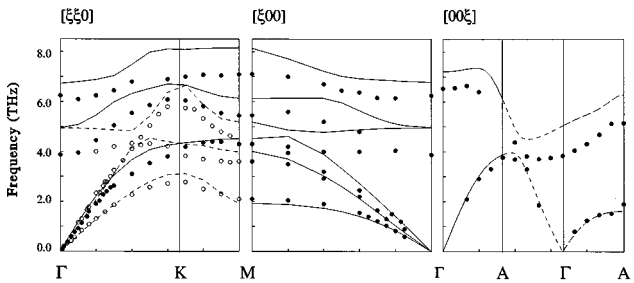

FIG. 7. Low-frequency phonon dispersion curves in the main directions of α-quartz as predicted by the KFBS potential in comparison with experiment. Experimental data, temperatures for which the calculations are done and symbols are the same as in Fig. 5.

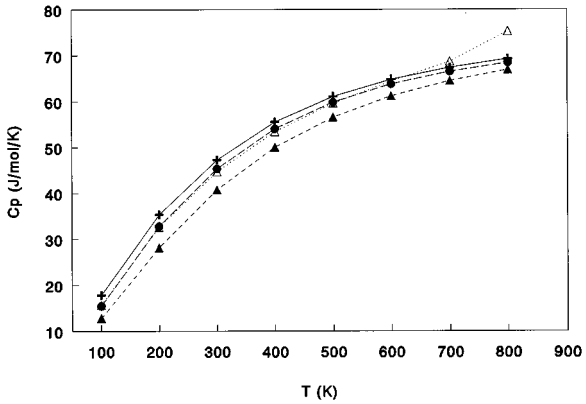

FIG. 8. Predictions for the constant pressure heat capacity of α-quartz versus temperature, compared with experimental data of Richet *et al.* (Ref. 37). Crosses: BJS predictions. Closed triangles: KFBS predictions. Closed points: JC predictions. Open triangles: experimental data.

accurate performance of the JC potential at higher pressures is due to underestimation of both the Si-O-Si bond angle and the OO repulsions at short interatomic distances. Therefore, we expect that the JC potential is less appropriate for the modeling of materials that are characterized by narrow Si-O-Si bond angles combined with short OO distances, which is the case for dense structures or materials that are subjected to high pressures. This is consistent with predictions of the JC potential for the structure and elasticity of the dense materials stishovite[12] and coesite,[39] which are less accurate than those of the other potentials. We expect that the JC potential is appropriate for the modeling of thermodynamic properties, low-frequency phonon dispersion curves, and the structure of materials which have a density lower than that of α-quartz. This is in line with accurate predictions of the structure,[11,32,47] low-frequency Raman and infrared spectra[40] of a large variety of silicates.

B. The KFBS potential

At low pressures and variable temperatures, the KFBS potential models the α-quartz structure less accurately than the JC potential. The KFBS prediction for the elastic constants at ambient conditions is accurate. The KFBS potential is less suitable for modeling low-frequency Raman modes at any pressure. Also, the phonon dispersion curves and thermodynamic properties of α-quartz at zero pressure are less accurately predicted. At high pressures, the KFBS prediction for the mechanical properties of α-quartz is accurate and the structure is predicted reasonably. Overestimation of the Si-O-Si bond angle is mainly responsible for the less accurate prediction of the structure, spectra, and thermodynamical properties of α-quartz. We have demonstrated that the overestimated stiffness of the Si-O-Si bond angle does not conflict with correct predictions for the mechanical behavior of α-quartz at high pressures. We expect the KFBS potential to be appropriate for high pressure studies on the structure and elasticity of dense silicates. This is in line with reasonable predictions for the structure and elasticity of stishovite[12] and coesite[39] at zero pressure and temperature. We expect that the KFBS potential would be less suitable for modeling the

structure and thermodynamic properties of materials having a density lower than that of α-quartz. This is consistent with less accurate predictions for the structure[41] and the low-frequency Raman and infrared spectra[40] of a large variety of all-silica polymorphs.

C. The BJS potential

The BJS prediction for the α-quartz structure is less accurate than both other potentials. This potential is able to model elasticity, thermodynamic properties, low-frequency Raman modes, and phonon dispersion curves of α-quartz at zero pressure. The BJS potential gives accurate predictions for the mechanical properties and the low-frequency Raman modes of α-quartz at high pressure. The less accurate prediction of the structure is mainly due to underestimation of both the Si-O-Si bond angle and the OO repulsions. The underestimated OO repulsions partially compensate for the too narrow Si-O-Si bond angle and therefore the BJS predictions for properties other than the structure are less affected. As the BJS potential is completely *ab initio*, there is no reason to believe that it should behave differently for other silica-polymorphs, which is supported by calculations at zero pressure and temperature for a large variety of silica-polymorphs.[10,41] We therefore expect the BJS potential to be appropriate for modeling thermodynamic and mechanical properties of silicates at variable pressures. In particular, the ability to model thermodynamic properties of silicates at high pressure is desirable. Our results indicate that this is not feasible with both other potentials. The BJS results indicate that both the OO repulsion and the interactions that govern the Si-O-Si bond angle must be stiffened. A modified version of the BJS potential with stiffened Si-O-Si bond angle interactions indeed gives better structure predictions for a large number of all-silica polymorphs, as has been shown elsewhere.[41] Further improvement of the BJS potential is subject of current research.

ACKNOWLEDGMENTS

This work has been supported by the Dutch Foundation for Chemical Research (SON) with financial aid from the Dutch Organization of Pure and Applied Research (NWO). One of us (K.d.B) thanks Dr. A. J. M. de Man for his kind assistance on the group theoretical decomposition of the phonon dispersion curves.

APPENDIX

Free-energy calculations require evaluation of the phonon frequencies for all wave vectors in the Brillouin zone. The frequencies are determined by taking only the frequencies on a three-dimensional grid in the Brillouin zone with an appropriate weighting factor.[42] Grids must be carefully chosen to avoid results that are determined by the number of **k** points used. To select an appropriate grid we did the following tests. Calculations have been done on α-quartz for several temperatures using the three potentials with a number of grids proposed by Fillipini *et al.*[42] and Pavesi *et al.*[43] We have varied for each grid the number of **k** points. We have checked uneven grids, which are more dense in the region of the Γ point, against equally spaced grids. We also tested the effect of sampling the whole or the half irreducible part of the Brillouin zone, because α-quartz is trigonal and therefore, in principle, the whole Brillouin zone should be sampled.[42] We found that the calculated constant pressure entropy varies the most with the use of a particular grid where variation in other properties is negligible at any temperature above $T=50$ K. For 125 points in **k** space at $T=300$ K the variation in the entropy with the above mentioned grids is less than 1%. This variation decreased at higher temperatures, due to the lower occupancy number of the phonons close to the Γ point. Furthermore, we carried out calculations at elevated temperature and pressure. The use of a dense grid is then mandatory for detecting imaginary frequencies that are due to pressure-induced mode softening. Hence we selected the following uneven 125-point grid in **k** space, with each of the three coordinates k_n having values:

$$k_n=\frac{3(2^{n-1})-2}{4(2^N-1)}. \tag{A1}$$

In Eq. (A1) N denotes the number of grid points in the reciprocal lattice and $n=1,2,\ldots,N$. For temperatures below 50 K all predicted properties vary too much with the number of **k** points in any used grid. This is caused by the strongly increasing acoustic modes near the Γ point which contribute the most at low temperatures. More elaborate schemes are then needed.[44] Therefore, we present results for temperatures above 100 K. Furthermore, the calculations do not include the Γ point, due to the singularity in the Ewald sum at $\mathbf{k}=0$. Hence we give Raman results obtained from calculations in the limit $\mathbf{k}\rightarrow 0$. Calculations have been done with this limit taken along the a and c axis of α-quartz.

[1] J. Chelikowsky, N. Troullier, J. L. Martins, and H. E. King, Phys. Rev. B **44**, 489 (1991).
[2] N. Binggeli, N. Troullier, J. L. Martins, and J. Chelikowsky, Phys. Rev. B **44**, 4771 (1991).
[3] N. Binggeli and J. Chelikowsky, Phys. Rev. Lett. **69**, 2220 (1992).
[4] N. R. Keskar and J. R. Chelikowky, Phys. Rev. B **46**, 1 (1992).
[5] N. Binggeli, N. R. Keskar, and J. R. Chelikowsky, Phys. Rev. B **49**, 3075 (1994).
[6] J. R. Chelikowsky and N. Binggeli, Comp. Mater. Sci. **2**, 111 (1994) and references therein.
[7] X. Gonze, J. C. Charlier, D. C. Allan, and M. P. Teter, Phys. Rev. B **50**, 13 035 (1994).
[8] C. Lee and X. Gonze, Phys. Rev. B **49**, 1686 (1994).
[9] C. Lee and X. Gonze, Phys. Rev. B **51**, 8610 (1995).
[10] K. de Boer, A. P. J. Jansen, and R. A. van Santen, Chem. Phys. Lett. **223**, 46 (1994).
[11] R. A. Jackson and C. R. A. Catlow, Mol. Simul. **1**, 207 (1988).
[12] G. J. Kramer, N. P. Farragher, B. W. H. van Beest, and R. A. van Santen, Phys. Rev. B **43**, 5068 (1991).
[13] S. Tsuneyuki, M. Tsukada, H. Aoki, and Y. Matsui, Phys. Rev. Lett. **61**, 869 (1988).

[14] S. C. Parker, computercode: PARAPOCS, BATHPROGS (School of Chemistry, University of Bath, Claverton Down, Bath BA2 7AY, U.K.)
[15] S. C. Parker and G. D. Price, Adv. Solid State Chem. **1**, 295 (1989).
[16] C. R. A. Catlow and M. J. Norgett (private communication).
[17] G. J. Kramer, A. J. M. de Man, and R. A. van Santen, J. Am. Chem. Soc. **113**, 6435 (1991).
[18] R. M. Hazen, L. W. Finger, R. J. Hemley, and H. K. Mao, Solid State Commun. **XX**, 507 (1989).
[19] L. Levien, C. T. Prewitt, and D. J. Weidner, Am. Mineral. **65**, 920 (1980).
[20] We compare predicted values for the Si-O-Si bond angle with experimental data of Glinneman *et al.* (Ref. 21), that were obtained for pressure between 0 and 10.2 GPa. Although Hazen *et al.* (Ref. 18) reported bond angles of α-quartz at pressures up to 12.5 GPa, we do not use these values in our comparison because they are less precise than the Glinneman data (Ref. 21). Calculated values for the c axis and c/a ratio are compared with both the Glinneman and Hazen data.
[21] J. Glinneman, H. E. King, Jr., H. Schultz, Th. Hahn, S. J. La Placa, and F. Dacol, Z. Kristallogr. **198**, 177 (1992).
[22] M. Born and K. Huang, in *Dynamical Theory of Crystal Lattices*, *The International Series of Monographs on Physics*, edited by D. H. Wilkinson and W. Marshall (Clarendon, Oxford, 1968).
[23] M. S. Somayazulu, S. M. Sharma, and S. K. Sikka, Phys. Rev. Lett. **73**, 98 (1994) and references therein.
[24] J. S. Tse and D. D. Klug, Phys. Rev. Lett. **67**, 3559 (1991).
[25] K. J. Kingma, R. J. Hemley, H. H. Mao, and D. R. Veblen, Phys. Rev. Lett. **70**, 3927 (1993).
[26] L. E. McNeil and M. Grimsditch, Phys. Rev. Lett. **72**, 1301 (1994).
[27] K. J. Kingma, R. J. Hemley, H. H. Mao, and D. R. Veblen, Phys. Rev. Lett. **72**, 1302 (1994).
[28] K. Kihara, Eur. J. Mineral. **2**, 63 (1990).
[29] R. J. Hemley, A. P. Jephcoat, H. K. Mao, L. C. Ming, and M. H. Manghnani, Nature **334**, 52 (1988).
[30] G. W. Watson and S. C. Parker, Philos. Mag. Lett. **71**, 59 (1995).
[31] W. Terhune, T. Kushida, and G. W. Ford, Phys. Rev. B **32**, 8416 (1985).
[32] P. Tschafeser, Ph.D. thesis, University of Bath, Bath, 1992.
[33] G. W. Watson, Ph.D. thesis, University of Bath, Bath, 1994.
[34] R. J. Hemley, in *High Pressure Research in Mineral Physics*, Geophys. Monogr. Ser. Vol. 39, edited by M. H. Manghnani and Y. Syono (AGU, Washington, D. C., 1987), pp. 347–359.
[35] K. J. Dean, W. F. Sherman, and G. R. Wilkinson, Spectrochim. Acta **38A**, 1105 (1982).
[36] R. J. Hill and G. V. Gibbs, Acta Crystallogr. B **35**, 25 (1978).
[37] P. Richet, Y. Bottinga, L. Denielou, J. P. Petit, and C. Tepui, Geoch. Cosmochem. Acta **46**, 2639 (1982).
[38] S. W. Kieffer, Rev. Geophys. Space Phys. **17**, 1 (1979).
[39] K. P. Schröder (private communication).
[40] A. J. M. de Man, Ph.D. thesis, Eindhoven University of Technology, Eindhoven, 1992.
[41] K. de Boer, A. P. J. Jansen, and R. A. van Santen, Phys. Rev. B **52**, 12 579 (1995).
[42] G. Filippini, C. M. Gramaccioli, M. Simonetta, and G. B. Suffritti, Acta Crysttallogr. A **32**, 259 (1979).
[43] A. Pavesi (private communication).
[44] T. H. K. Barron and A. Pasternak, J. Phys. Solid State Phys. **20**, 215 (1987).
[45] H. J. McSkimin, P. Andreat, Jr., and R. N. Thurston, J. Appl. Phys. **36**, 1524 (1965).
[46] Q. Wang, G. A. Saunders, E. F. Lambson, P. Tschaufeser, S. C. Parker, and B. J. James, Phys. Rev. B **45**, 10 242 (1992).
[47] Q. Wang (unpublished).
[48] B. Dorner, H. Grimm, and H. Rzany, J. Phys. C **13**, 6607 (1980).
[49] D. Strauch and B. Dorner, J. Phys. Condens. Matter **5**, 6149 (1993).